Electrochemical Science Advances

Chemistry Europe
European Chemical Societies Publishing

RESEARCH ARTICLE OPEN ACCESS

Enhanced Electrochemical Performance of Supercapacitors Using Fe_3O_4-Doped Biomass-Derived Activated Carbon Electrodes

Kadir Sinan Aslan[1] | Erdal Ertaş[2] | Mehmet Firat Baran[2] | Abdulkadir Levent[3] | Şeyhmus Tümür[4] | Aziz Eftekhari[5] | Ondrej Šauša[6,7] | Oleh Smutok[8] | Taras Kavetskyy[6,9] | Evgeny Katz[8]

[1]Department of Biology, Faculty of Science, Dicle University, Diyarbakir, Turkey | [2]Department of Food Technology, Vocational School of Technical Sciences, Batman University, Batman, Turkey | [3]Department of Chemistry, Faculty of Arts and Sciences, Batman University, Batman, Turkey | [4]Faculty of Engineering, Dicle University, Diyarbakir, Turkey | [5]Department of Biochemistry, Faculty of Science, Ege University, Izmir, Turkey | [6]Institute of Physics, Slovak Academy of Sciences, Bratislava, Slovakia | [7]Department of Nuclear Chemistry, FNS, Comenius University, Bratislava, Slovakia | [8]Department of Chemistry and Biochemistry, Clarkson University, Potsdam NY, USA | [9]Department of Physics and Information Systems & Department of Biology and Chemistry, Drohobych Ivan Franko State Pedagogical University, Drohobych, Ukraine

Correspondence: Taras Kavetskyy (kavetskyy@yahoo.com) | Evgeny Katz (ekatz@clarkson.edu)

Received: 25 July 2025 | **Revised:** 30 September 2025 | **Accepted:** 6 October 2025

Keywords: activated carbon | anode materials | biomass-derived nanocomposites | electrochemical performance | magnetic Fe_3O_4 nanoparticles | supercapacitors

ABSTRACT

The energy storage performance of supercapacitors—defined by specific capacitance, energy density, and power density—is strongly influenced by the structural and electrochemical properties of electrode materials. While cathode development has advanced significantly, research on efficient and sustainable anode materials remains limited, hindering further improvements in energy density. This study presents a low-cost, sustainable anode material derived from *Abelmoschus esculentus* (AE) seed biomass. Activated carbon (AE-AC) was prepared via chemical activation and subsequently coated with magnetic Fe_3O_4 nanoparticles synthesised through co-precipitation to form an AE-AC-doped Fe_3O_4 nanocomposite. The materials were characterised using XRD, SEM–EDX, BET surface area analysis, and other techniques. Electrochemical performance was evaluated using cyclic voltammetry (CV), galvanostatic charge/discharge (GCD), and electrochemical impedance spectroscopy (EIS). At a scan rate of 2.5 mV/s, both electrodes exhibited peak capacitance. GCD analysis showed specific capacitances of 119.97 F/g for AE-AC and 205.86 F/g for AE-AC-doped Fe_3O_4 at 0.05 A/g. EIS results confirmed enhanced performance of the nanocomposite in acidic medium. These findings highlight the potential of AE-based activated carbon composites as environmentally friendly and efficient anode materials for next-generation supercapacitors.

1 | Introduction

The combined challenges of climate change driven by global warming, the projected depletion of fossil fuel reserves, the ongoing energy crisis, and rising environmental pollution have made the development of sustainable and eco-friendly energy sources an urgent priority [1, 2]. At the same time, the rapid advancement of portable electronic devices and the growing demand for stable electrochemical energy conversion and storage systems underscore the need for high-performance, lightweight, and flexible energy storage technologies that can efficiently utilise renewable energy resources. Additionally, supercapacitors have

This is an open access article under the terms of the Creative Commons Attribution License, which permits use, distribution and reproduction in any medium, provided the original work is properly cited.

© 2025 The Author(s). *Electrochemical Science Advances* published by Wiley-VCH GmbH.

emerged as promising candidates for storing electrochemical energy that can be used in wearable electronic devices [3–6].

Supercapacitors have attracted significant attention in recent years because they can compensate for the shortcomings of traditional capacitors and batteries due to their advantages of fast charge and discharge, high energy density, and long cycle life compared to batteries and other common capacitors. A review of recent literature reveals a growing research focus on the use of supercapacitors [7], their dimensions [8], high power density [9], charge-discharge capacity [10], flexibility and specific capacitance [11], improvement of various electrochemical performances [12], electrode preparation and device configuration [13].

Supercapacitors are divided into three groups based on how they store energy: electrical double-layer capacitors (EDLC), pseudocapacitors, and hybrid capacitors. EDLCs store energy by physically accumulating charges at the interface between the electrode and the electrolyte, without involving any chemical reactions. Pseudo-capacitors store energy through rapid and reversible chemical (redox) reactions occurring on the electrode surface. Hybrid capacitors possess the properties of both structures. These devices utilise two different electrode materials, one double-layered and the other pseudocapacitive, to achieve both high power and high energy density [14–16]. Due to the supercapacitance mechanism, pseudocapacitors have a higher specific capacitance value than EDLC-type capacitors [17].

Supercapacitors are basically divided into two main categories based on their energy storage mechanism: electric double layer capacitors (EDLCs) and pseudocapacitors [18]. Energy storage in EDLC-type capacitors occurs through the electrostatic charge separation mechanism occurring at the electrode and electrolyte interface. This mechanism is supported by the use of carbon-based materials with large surface areas, such as carbon nanotubes (CNTs), activated carbon (AC), and graphene [19]. Although EDLCs offer advantages such as fast charge/discharge properties and long cycle life thanks to this structure, they are capacitors with generally low specific capacitance values because they are limited to only physical charge separation [20]. Pseudocapacitors, on the other hand, store energy through fast and reversible redox (faradic) mechanisms occurring on the surface or in the volume of the electrode material. This mechanism is made possible by the use of electrochemically active nano-sized materials such as transition metal oxides and their hydroxides, which can offer a large number of functional sites [21]. Metal oxides and their hydroxyl structures, such as CuO [22], Co_3O_4 [23], MoO_2 [24], V_2O_5 [25], NiO [26], MnO_2 [27], $Co(OH)_2$ [28], $Ni(OH)_2$ [29], Fe_2O_3 [30] and Fe_3O_4 [31], are commonly used for pseudocapacitive materials. Compared to the materials used in EDLC-type capacitors, these materials offer significantly higher specific capacitance and energy density. However, given the redox processes involved, both cycling stability and speed performance in these types of supercapacitors are generally limited [32].

Magnetite (Fe_3O_4) has significant potential as a pseudocapacitive electrode material due to its environmental sustainability, abundance in nature, low production cost, and variable oxidation states that allow multivalent transitions between Fe^{2+}/Fe^{3+} ions. These properties make Fe_3O_4 a cost-effective and promising material candidate for environmentally friendly energy storage technologies that can provide high specific capacitance values [33–35].

With the increasing demand for energy storage systems today, the development of environmentally friendly, low-cost, and high-performance electrode materials has gained significant importance. In this context, biomass-based carbon materials have become extremely attractive because they can be obtained from abundant, renewable, and sustainable resources [36]. In particular, the recycling of agricultural wastes and their conversion into high surface area activated carbons offers an important solution for environmental waste management and constitutes a viable alternative for the production of materials for economical energy storage [37]. It has been shown in the literature that supercapacitor performance can be significantly improved by modifying activated carbon with various metal oxides, especially compounds such as Fe_3O_4, which have electroactive properties [38].

This study presents activated carbon (AE-AC) derived from okra seed waste as a sustainable electrode material. To enhance performance, an AE-AC-doped Fe_3O_4 nanocomposite was prepared, and their electrochemical behaviours were comparatively evaluated in supercapacitor applications. The work highlights the potential of converting agricultural waste into value-added, eco-friendly materials for next-generation energy storage devices.

2 | Results and Discussion

2.1 | SEM Analysis of AE-AC and AE-AC-Doped Fe_3O_4 Nanocomposites

The surface morphology of the AE-AC material and the AE-AC doped Fe_3O_4 nanocomposite were investigated using scanning electron microscopy (SEM). Figure 1a presents the SEM image of the AE-AC material, while Figure 1b shows the SEM image of the AE-AC doped Fe_3O_4 nanocomposite.

The SEM image in Figure 1a illustrates the microstructure of pure activated carbon derived from AE seeds, revealing a porous, irregular, and spongy texture [39]. In contrast, Figure 1b presents the morphology of the AE-AC-doped Fe_3O_4 nanocomposite after Fe_3O_4 nanoparticles have been deposited on its surface. The structure of this nanocomposite shows a noticeable transformation: the previously porous surface becomes denser, more clustered, and amorphous, with the original porosity disappearing. This increased particle accumulation on the surface reflects the coating effect, which leads to a more compact and homogeneous morphology of the nanocomposite, as the magnetic nanoparticles form a tightly bound structure [40].

2.2 | EDX Analysis of AE-AC and AE-AC-Doped Fe_3O_4 Nanocomposites

The surface elemental composition of the AE-AC material and the AE-AC-doped Fe_3O_4 nanocomposite was characterised using energy-dispersive X-ray (EDX) analysis. Figure 2 presents the EDX spectra of both the AE-AC material and the AE-AC-doped Fe_3O_4 nanocomposite.

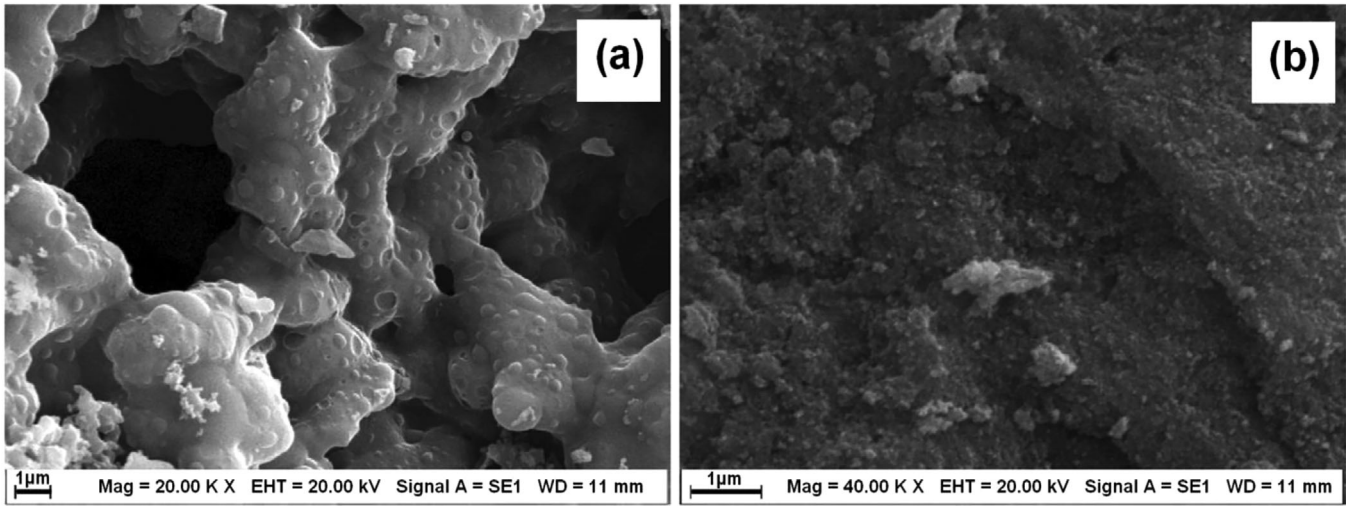


FIGURE 1 | SEM images of (a) AE-AC and (b) AE-AC-doped Fe_3O_4 nanocomposites.

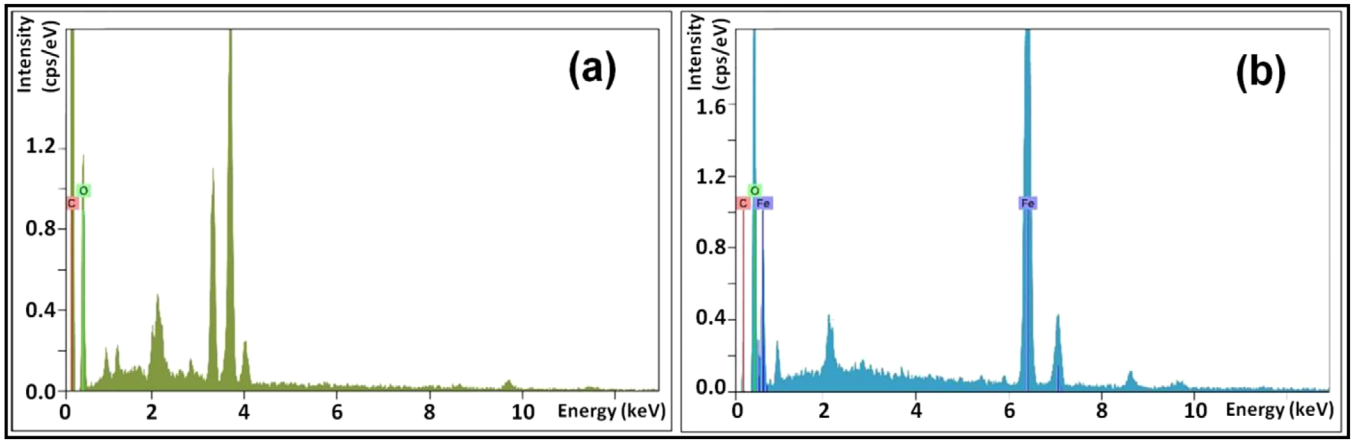


FIGURE 2 | EDX images of (a) AE-AC and (b) AE-AC-doped Fe_3O_4 nanocomposites.

EDX analysis results showed that it contained carbon (45.69%), oxygen (44.77%), calcium (5.05%), potassium (2.16%), zinc (1.96%), and magnesium (0.36%), indicating that the AE-AC material containing impurities was successfully synthesised (Figure 2a). In contrast, when the elemental composition of the synthesised AE-AC-doped Fe_3O_4 nanocomposite was examined, EDX analysis confirmed that it contained carbon (9.43%), oxygen (49.91%), and iron (40.67%), indicating the successful synthesis of the AE-AC-doped Fe_3O_4 nanocomposite (Figure 2b). Although not indicated in the spectrum, the presence of elements other than C, O, and Fe may correspond to trace amounts of impurities (such as zinc and calcium) remaining on the particle surface after washing [41].

EDX, BET, and XRD analyses indicate that the AE-AC material has a large surface area (86.88 m^2/g) due to its high carbon and oxygen content, and these properties enhance electrochemical performance. In the AE-AC-doped Fe_3O_4 nanocomposite, XRD confirms the crystalline structure of Fe_3O_4, while the iron content (40.67%) improves magnetic and conductive properties. However, the addition of Fe_3O_4 reduces the BET surface area to 20.78 m^2/g, reducing porosity and improving stability, although it reduces energy storage capacity.

2.3 | XRD Analysis of AE-AC and AE-AC-Doped Fe_3O_4 Nanocomposites

The characterisation results obtained from XRD analysis (Figure 3) indicate that the activated carbon is amorphous, as evidenced by a broad diffraction peak (Figure 3a). The peaks of the AE-AC-doped Fe_3O_4 nanocomposite revealed the characteristic diffraction signals of Fe_3O_4 at 2θ values of 30.2°, 35.6°, 43.3°, 52.8°, 57.2°, and 62.9°. These peaks correspond to the cubic spinel structure of Fe_3O_4, and can be indexed to the (220), (311), (400), (422), (511), and (440) planes, respectively, based on the 2θ values and their relative intensities. Furthermore, the sharpening and intensification of these peaks in the nanocomposite confirm the successful formation of the AE-AC-doped Fe_3O_4 nanocomposite (Figure 3b) [42, 43].

2.4 | BET Analysis of AE-AC and AE-AC-Doped Fe_3O_4 Nanocomposites

The effective surface area of active electrode materials is considered an important parameter determining the electrochemical performance of supercapacitors. In this study, the BET surface

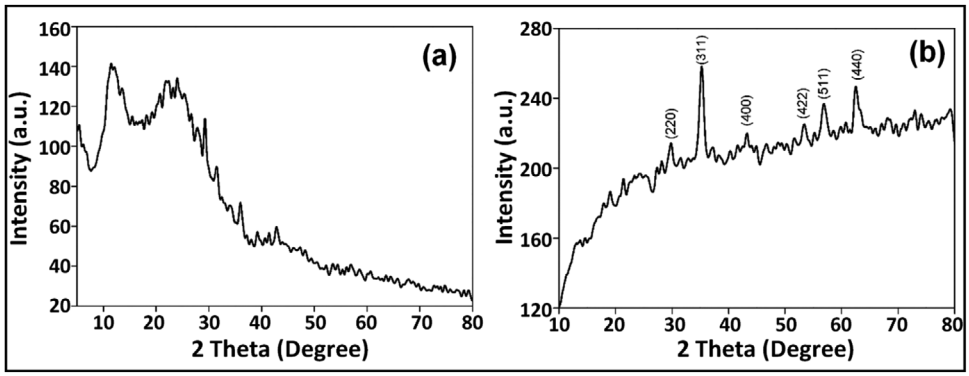


FIGURE 3 | XRD images of (a) AE-AC vs. (b) AE-AC-doped Fe_3O_4 nanocomposites.

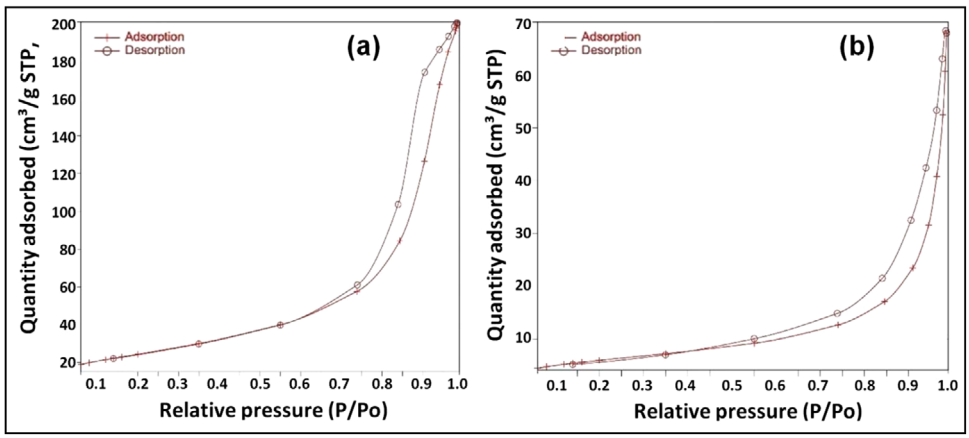


FIGURE 4 | The N_2 adsorption-desorption isotherms of (a) AE-AC and (b) AE-AC-doped Fe_3O_4 nanocomposites.

area and porosity properties of the AE-AC material and the AE-AC-doped Fe_3O_4 nanocomposite were systematically analysed using a Micromeritics Gemini VII 2390 Series Surface Area Analyser. The obtained N_2 adsorption-desorption isotherms are presented in Figure 4 to evaluate the pore structure and surface properties of both materials in detail. The BET surface area of the AE-AC material was measured to be approximately 86.88 m^2/g, with a total pore volume of 0.3046 cm^3/g and an average pore diameter of 140.23 Å. These values suggest that the material possesses a large surface area, which is conducive to high charge-discharge performance and enhanced energy density. However, the BET surface area of the AE-AC-doped Fe_3O_4 nanocomposite was measured as 20.78 m^2/g, the total pore volume as 0.0938 cm^3/g, and the average pore diameter as 180.56 Å. The Fe_3O_4 coating covered a large portion of the AE-AC surface, reducing the effective surface area and causing significant changes in the pore structure. The settlement of Fe_3O_4 particles in the pores of the AE-AC material resulted in a decrease in the surface area and an increase in the pore diameter. In addition, the narrow hysteresis loop observed for both materials indicates the presence of micro- and mesoporous structures, suggesting that the Fe_3O_4 doping may have partially modified this structure. As a result, changes in the surface area and pore structure of the Fe_3O_4 coating AE-AC material may affect the electrochemical performance of supercapacitors, and the possible improvement or deterioration in this performance may vary depending on the characteristics of the material structure and composite formation [44, 45].

2.5 | Electrochemical Properties of AE-AC and AE-AC-Doped Fe_3O_4 Nanocomposites

2.5.1 | Cyclic Voltammetry (CV) Analysis

The current-potential behaviour of the supercapacitor electrodes and the reversibility of the charge storage mechanism were investigated in detail by the CV technique. Experimental studies were carried out in a 1 M H_2SO_4 aqueous electrolyte medium. Voltammograms obtained at scan rates between 2.5 mV/s and 100 mV/s are presented in Figure 5a and Figure 5b. Both electrode materials, AE-AC and AE-AC-doped Fe_3O_4, reached their highest specific capacitance values at a scan rate of 2.5 mV/s. Specific capacitance values for all scan rates are given in Table 1. It was observed that AE-AC-doped Fe_3O_4 electrodes exhibited higher specific capacitance values compared to AE-AC at each scan rate. The CVs of AE-AC and AE-AC-doped Fe_3O_4 electrodes are presented in Figure 5. To facilitate direct comparison, all scans were started from the same initial potential. We note that experiments performed on AE-AC at potentials more negative than −0.20 V exhibited a substantial and rapidly increasing residual (charging/back-current) signal, which became more pronounced as the scan rate increased. This excessive residual current affects reproducibility and masks faradaic features; therefore, the comparative CV data discussed below were acquired and analysed in the −0.20 V to +1.20 V range, which provided the most reproducible and reliable responses for both electrodes.

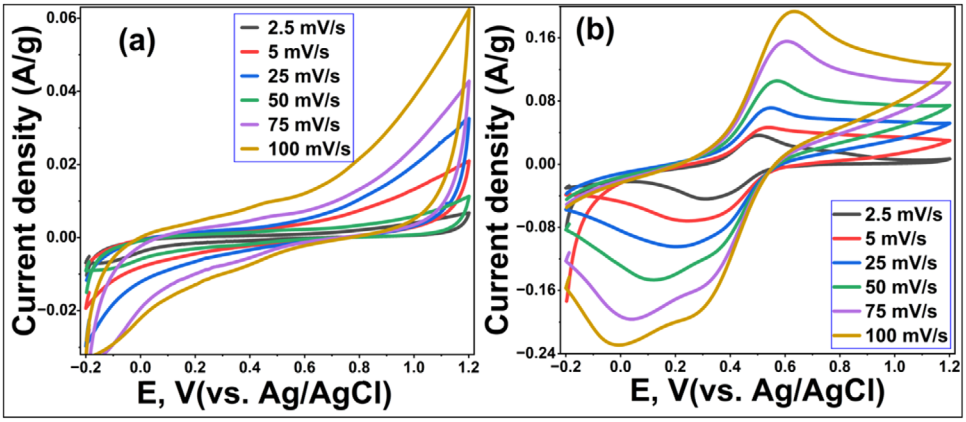


FIGURE 5 | Comparison of CV curves for **(a)** AE-AC and **(b)** AE-AC-doped Fe_3O_4 nanocomposites in 1 M H_2SO_4 at a scan rate of 10 mV/s.

TABLE 1 | Specific capacitance of AE-AC and AE-AC-doped Fe_3O_4 electrodes at varying scan rates in H_2SO_4.

Scan rate (mV/s)	AE-AC (F/g)	AE-AC-doped Fe_3O_4 (F/g)
2.5	20.78	128.42
5	15.08	127.06
25	6.02	35.32
50	2.92	24.40
75	2.88	22.80
100	1.19	20.68

As shown in Figure 5b, the doped electrode exhibits two distinct reduction features. The first is a broad reduction peak centred at approximately +0.25 V, which appears broadened and of lower current density, while a second, more distinct reduction peak is observed near 0.0 V. The relative breadth and intensity of these peaks suggest overlapping or sequential reduction processes, with the broader +0.25 V feature likely arising from a surface-confined or composite-related process and the sharper ~0.0 V peak corresponding to a more well-defined redox transition. These reversible reactions are an indication of faradaic processes occurring with the contribution of electroactive functional groups in the material, and these redox couples were also clearly observed in the GCD curves (Figure 6a and Figure 6b). These findings support the successful doping of Fe_3O_4 into the AE-AC structure and its electrochemical activity. This is also consistent with data obtained from other characterisation techniques. A decrease in specific capacitance values was observed for both electrodes with increasing scan speed. This decrease can be attributed to limited charge transfer due to the inability of ions to sufficiently diffuse to the electrode surface and into the pores at high scan rates. Similarly, in GCD experiments, it was observed that specific capacitance values decreased as the current density increased (Figure 6). This behaviour can be attributed to faradaic effects caused by the electroactive functional groups present in the system. Furthermore, the change in specific capacitance values with scan rate reflects the effect of the material's pore structure on ion transport. This observation is a characteristic behaviour widely reported in the literature for materials exhibiting supercapacitor properties [4, 46].

2.5.2 | Galvanostatic Charge/Discharge (GCD) Analysis

The GCD method provides important information in evaluating the supercapacitor behaviour of electrode materials, especially regarding the reversibility and electrochemical stability of the charge storage process. In this study, GCD analyses of electrodes designed from AE-AC and AE-AC-doped Fe_3O_4 activated carbon

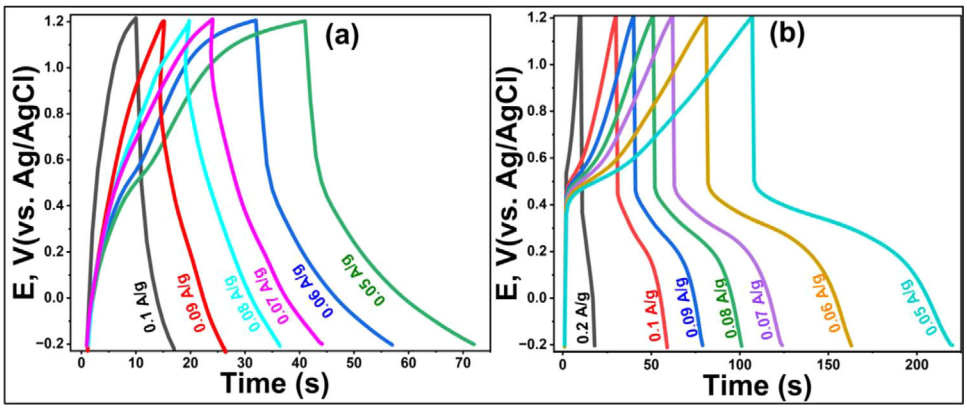


FIGURE 6 | Comparative GCD analysis of **(a)** AE-AC and **(b)** AE-AC-doped Fe_3O_4 at various current densities in 1 M H_2SO_4.

TABLE 2 | Current density-dependent specific capacitance values of AE-AC and AE-AC-doped Fe_3O_4 in 1 M H_2SO_4 via GCD analysis.

Current density (A/g)	AE-AC (F/g)	Current density (A/g)	AE-AC-doped Fe_3O_4 (F/g)
0.05	119.97	0.05	205.86
0.06	115.82	0.06	174.89
0.07	111.98	0.07	153.03
0.08	108.78	0.08	145.74
0.09	71.98	0.09	65.58
0.10	55.91	0.10	36.44
		0.20	29.15

materials were carried out in the potential range of -0.2 V to +1.2 V in a 1 M H_2SO_4 environment. Experiments were carried out at different current densities ranging from 0.05 A/g and 0.10 A/g for the AE-AC electrode and between 0.05 A/g and 0.20 A/g for the AE-AC-doped Fe_3O_4. The GCD curves presented in Figure 6 and the specific capacitance (C_{sp}) values calculated according to the formulas given in the Method section are shown in Table 2. It has been observed that the addition of magnetic Fe_3O_4 to activated carbon enhances the faradaic contribution by increasing the formation of electroactive functional groups on the surface of activated carbon. This caused the IR (ohmic resistance induced) drop to be more pronounced in Fe_3O_4-doped AE-AC compared to AE-AC, and therefore a faster decrease in specific capacitance values with increasing current density (Figure 6 and Table 2). Under the most favourable experimental conditions, defined as measurements performed in 1 M H_2SO_4 at a current density of 0.05 A/g, the AE-AC electrode reached a specific capacitance of 119.97 F/g, whereas the AE-AC-doped Fe_3O_4 electrode exhibited a higher value of 205.86 F/g under the same conditions. It was clearly observed that the specific capacitance values decreased with increasing current density for both electrode materials. This decrease is attributed to the inability of electrolyte ions to adequately penetrate the interior of the porous structure, particularly at high current densities [6, 46, 47].

In order to evaluate the cyclic stability of the electrodes, the cycling performances of AE-AC (Figure 7a) and AE-AC-doped Fe_3O_4 (Figure 7b) supercapacitors were tested in 1 M H_2SO_4 electrolyte at current densities of 0.10 A/g and 0.20 A/g, respectively. After 1000 cycles, AE-AC retained 91.34% of its initial capacitance, while AE-AC-doped Fe_3O_4 retained 88.20%, demonstrating good cycling stability for both materials.

These values indicate that both electrode materials have good cycling stability. As a result of energy and power density calculations, the AE-AC electrode exhibited an energy density of 3.98 Wh/kg and a power density of 1000 W/kg, while the AE-AC doped Fe_3O_4 electrode reached an energy density of 10.40 Wh/kg and a power density of 3500 W/kg (Figure 8). For both materials, a decreasing trend in energy density was observed as current density increased, suggesting that energy efficiency decreased as power output increased. This characteristic is consistent with typical electrochemical capacitor behaviour and supports the inclusion of both electrodes in the supercapacitor class [48].

2.6 | Electrochemical Impedance Spectroscopy (EIS) Measurement

The impedance data obtained are presented in the form of Nyquist diagrams and fitted with curves using the [R([RW]Q)T]

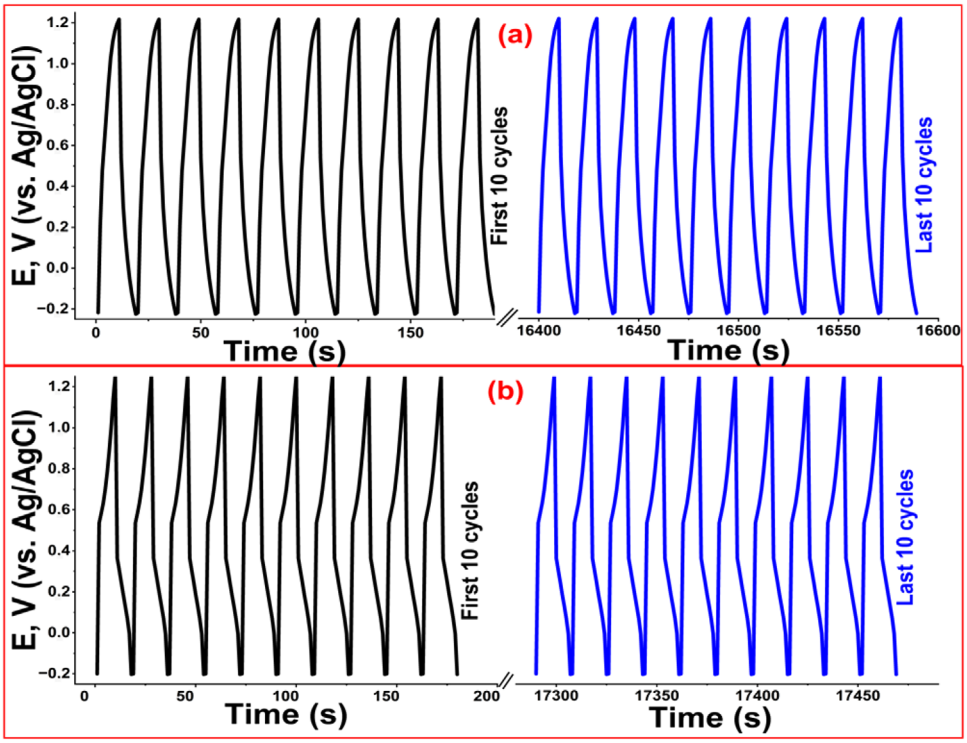


FIGURE 7 | Long-Term GCD cycling performance of **(a)** AE-AC and **(b)** AE-AC-doped Fe_3O_4 electrodes in 1 M H_2SO_4 acidic medium.

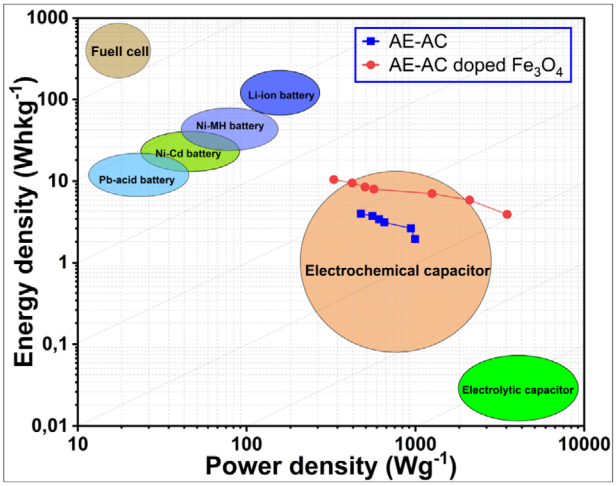


FIGURE 8 | Ragone plots comparing the energy and power densities of AE-AC and AE-AC-doped Fe_3O_4 electrodes.

equivalent circuit model, as illustrated in the inset of Figure 9a. In these diagrams, a semicircle representing the charge-transfer resistance (Rct) of the electrode is observed in the high-frequency region, while a warped sloped line representing the capacitive behaviour of the electrode is observed in the low-frequency region (Figure 9). It is stated in the literature that the Nyquist curve of an ideal supercapacitor is expected to show a line between the angles of 45° (Warburg diffusion) and 90° (ideal capacitive behaviour) with the imaginary axis. Deviations from this ideal geometry are generally related to the pore size distribution in the electrode, the ion diffusion depth, and the faradaic (pseudo-capacitive) reactions taking place at the surface. In addition, the ohmic potential drop observed at the beginning of the discharge process in the GCD curves is associated with faradaic processes caused by the functional groups present on the electrode surface. In an ideal, fully reversible supercapacitor, the GCD curves would be expected to be in the shape of an isosceles triangle. However, the reversible redox couples observed in the AE-AC doped Fe_3O_4 capacitor and the charge/discharge breaks in the GCD curves indicate that faradaic interactions are influential in the system. According to EIS analyses performed in acidic media, the equivalent series resistances of the AE-AC and AE-AC doped Fe_3O_4 capacitors were found to be 525 Ω and 152 Ω, respectively (Figure 9a). Furthermore, the specific capacitance values calculated in the 100 kHz to 0.1 Hz frequency range were determined using the equations given in the method section and were determined to be 22.32 F/g for AE-AC and 109.05 F/g for F AE-AC doped Fe_3O_4.

When the data in Figure 9b is examined in detail, it is seen that the specific capacitance values of the AE-AC doped Fe_3O_4 capacitor decrease sharply at low frequencies, followed by a plateau with no significant change at higher frequencies. This behaviour indicates that electrolyte ions are unable to diffuse sufficiently into the activated carbon pores, especially in the medium and high-frequency ranges [49]. In the AE-AC capacitor, no significant variation in capacitance values was observed as frequency increased.

When the Bode diagrams are evaluated, it is seen that the resistance values of the AE-AC capacitor at low frequencies are higher than those of the AE-AC-doped Fe_3O_4 capacitor. This indicates that both capacitors exhibit capacitive behaviour. However, both electrode systems exhibit deviations from the ideal capacitive response. These deviations are due to the mesoporous structure of the activated carbon used [50]. Consequently, it can be said that the AE-AC capacitor behaves like a double-layer capacitor in acidic environments, while the AE-AC-doped Fe_3O_4 behaves like a pseudocapacitor.

2.7 | Comparison of the Specific Capacitance of Different Supercapacitor Electrodes

Table 3 shows the highest specific capacitances obtained from CV at a scan rate of 2.5 mV/s for AE-AC and AE-AC-doped Fe_3O_4, measured as 119.97 and 205.86 F/g, respectively. They exhibit quite interesting and superior properties compared to other activated carbon and activated carbon-doped materials reported in the literature. Aruchamy et al. [51] reported a specific capacitance value of 103 F/g for $ZnMn_2O_4$/MWCNT. Gouda et al. [52] reported a specific capacitance value of 105 F/g for an AC

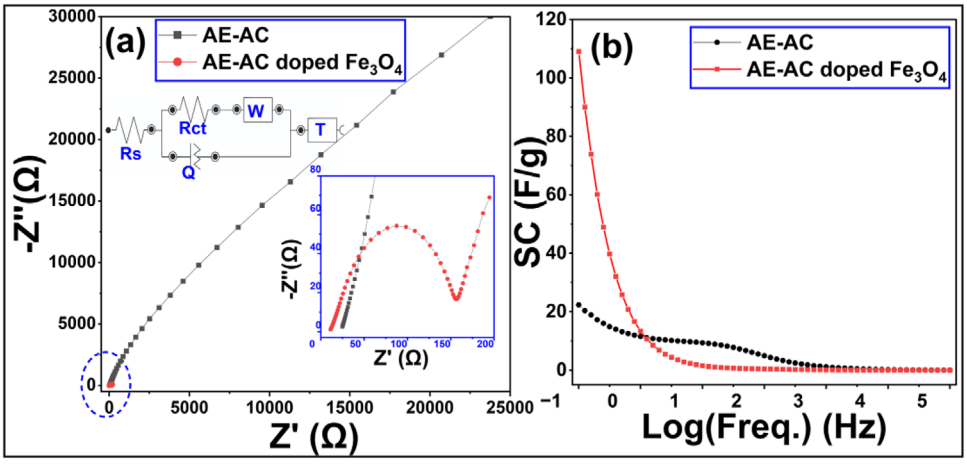


FIGURE 9 | Nyquist **(a)** and Bode **(b)** plots illustrating the effect of Fe_3O_4 incorporation on the electrochemical impedance behaviour of AE-AC and AE-AC-doped Fe_3O_4 electrodes in 1 M H_2SO_4.

TABLE 3 | Comparison of specific capacitance of different AE-AC vs. AE-AC-doped Fe_3O_4 nanocomposite electrode materials.

Electrode materials	Specific capacitance (C_s) (F/g)	Reference
$ZnMn_2O_4$/MWCNT	103	[51]
AC	105	[52]
Magnetic-activated carbon	76.23	[53]
Activated carbons (ACs)	84	[54]
CHAC	130	[55]
Fe_2O_3/CNT composite	54	[56]
CNT/Fe_3O_4	117.2	[57]
AE-AC	119.97	This work
AE-AC-doped Fe_3O_4	205.86	

electrode obtained from willow catkin (WC). Ozpinar et al. [53] reported a maximum specific capacitance of 76.23 F/g for the magnetic-activated carbon electrode obtained from hazelnut shell waste by phosphoric acid activation. Adan-Mas et al. [54] reported a specific capacitance value of 84 F/g for the activated carbon (AC) electrode obtained from coffee-derived biowastes. Raj et al. [55] reported a specific capacitance value of 130 F/g for the activated carbon electrode obtained from the agricultural waste cornhusk (CHAC). Xu et al. [56] reported a specific capacitance value of 54 F/g for the Fe_2O_3/CNT composite electrode. These results demonstrate that AE-AC and AE-AC-doped Fe_3O_4 have advantageous long-term electrochemical stability. This excellent performance can be attributed to the strong interaction between the AE-AC materials and the AE-AC-doped Fe_3O_4 nanocomposite, which prevents microstructure degradation during the reduction reaction.

3 | Conclusion

In this study, AE-AC-doped Fe_3O_4 nanocomposites were successfully synthesised by coating magnetic Fe_3O_4 nanoparticles onto activated carbon (AE-AC), which was derived via chemical activation of okra (*Abelmoschus esculentus*) seed biomass. Structural and morphological analyses using XRD, SEM, EDX, and BET confirmed the effective integration of Fe_3O_4 into the AE-AC matrix.

Electrochemical characterisation of AE-AC and AE-AC-doped Fe_3O_4 electrodes was conducted using CV, GCD, and EIS techniques in 1 M H_2SO_4 electrolyte. CV measurements revealed high capacitive behaviour for both electrodes, with maximum specific capacitance values obtained at a scan rate of 2.5 mV/s. GCD analysis showed a notable enhancement in specific capacitance from 119.97 F/g for AE-AC to 205.86 F/g for the AE-AC-doped Fe_3O_4 at 0.05 A/g. EIS results further supported this improvement, yielding specific capacitance values of 22.32 F/g and 109.05 F/g for AE-AC and AE-AC-doped Fe_3O_4, respectively, indicating better ion transport and lower internal resistance in the doped system. Long-term cycling tests demonstrated excellent stability, with capacity retention of 91.34% for AE-AC and 88.20% for AE-AC-doped Fe_3O_4 after 1000 cycles. Ragone plot analysis revealed higher energy and power densities for the Fe_3O_4-doped system (10.40 Wh/kg and 3500 W/kg) compared to AE-AC (3.98 Wh/kg and 1000 W/kg), attributed to the improved interfacial and structural properties introduced by Fe_3O_4 doping. Electrochemical analyses confirmed that AE-AC exhibits double-layer capacitive behaviour, while AE-AC-doped Fe_3O_4 displays pseudocapacitive characteristics due to faradaic interactions introduced by the Fe_3O_4 nanoparticles. These interactions significantly enhanced charge storage capacity and energy performance.

Overall, both AE-AC and AE-AC-doped Fe_3O_4 are promising low-cost, environmentally friendly, and sustainable electrode materials for supercapacitor applications. In particular, AE-AC-doped Fe_3O_4 stands out as a strong candidate for future energy storage technologies, offering superior specific capacitance, energy density, and cycling stability.

4 | Experimental

4.1 | Materials

4.1.1 | Chemicals

The analytically pure components, which were acquired from Sigma-Aldrich (Merck KGaA; Darmstadt, Germany), include ferrous chloride tetrahydrate ($FeCl_2{\cdot}4H_2O$), ferric chloride hexahydrate ($FeCl_3{\cdot}6H_2O$), hydrochloric acid (HCl), sodium hydroxide (NaOH), sulphuric acid (H_2SO_4), ammonium hydroxide (NH_4OH), potassium chloride (KCl) and zinc chloride ($ZnCl_2$). During the research, deionised water was used in the synthesis of the nanomaterial, preparation of the necessary solutions, and other processes.

4.1.2 | Synthesis of AE-AC

The seed part of the *Abelmoschus esculentus* (AE) plant was first washed with tap water and then cleaned by washing several times with ultrapure water to eliminate possible dust and contaminants. After the cleaning process was completed, the AE seeds were left to dry for 3 days in a sterile oven set at 30°C. The dried seeds were ground into powder using an IKA M20 Universal mill. The powdered sample was then stored under dry conditions in the dark to produce AEactivated carbon (AE-AC). Twenty grams of powdered *Abelmoschus esculentus* plant seeds were weighed and transferred to a 500 mL conical flask. 1 M zinc chloride solution was added, and stirring continued overnight at 75°C. The resulting mixture was then cooled to room temperature in the laboratory and then washed several times with ultrapure water to remove unreacted substances. After the washing process, the obtained product was dried at 100°C, and the powder sample was placed in a porcelain crucible and subjected to carbonisation for 2 h in a muffle furnace set at 500°C. After the carbonisation process, the product in the crucible was left to cool in the laboratory environment and then washed several times with 0.1 M HCl solution prepared with the help of a centrifuge to remove the remaining zinc, chlorine and other ions that remained in the environment without reacting. After the acid washing process, it was washed several times with ultrapure water to neutralise the

pH of the product, then dried in a lyophiliser and stored in a dark environment where appropriate conditions were provided for use in other synthesis steps and characterisation studies [58–60].

4.1.3 | Synthesis of AE-AC-Doped Fe_3O_4

For the synthesis of Fe_3O_4 coated with AC obtained from the seeds of the AE plant, methodological modifications were made to the traditional protocols in the literature; these modifications improved the morphological, structural, and functional properties of the compound by optimising parameters such as material coating rates, reaction times, and temperature control [61]. As the first step, 2.0 g of iron (III) chloride hexahydrate was added to a 100 mL three-necked flask containing 50 mL of ultrapure water and stirred with a magnetic stirrer at 800 rpm at room temperature for 15 min. In order to prevent oxidation of iron(III) ions in the solution, 5 drops of concentrated hydrochloric acid solution were slowly added to the solution while stirring. At the end of this period, after 2.10 g of iron (II) chloride tetrahydrate was added to the solution containing iron (III) ions, the temperature of the mixture was gradually increased to 90°C, and stirring continued for 30 min on a magnetic stirrer at 1000 rpm. As a second step, 20 mL of 26% NH_4OH solution was slowly added to the mixture, causing the iron salts in this medium to precipitate together, resulting in the black product. After the addition of the ammonia solution, the mixture was stirred for another 30 min at 90°C and 1000 rpm. As a third step, a solution of 0.5 g of AE-AC in 100 mL of water was added to the mixture under the same conditions and stirred for 1 h. After the specified time, the mixing system was shut down and allowed to cool to room temperature. After the cooling process, the synthesised AE-AC-doped Fe_3O_4 nanocomposite was separated from the mixing medium using a neodymium magnet [41, 62–63]. The resulting Fe_3O_4-AE-AC nanocomposite was washed several times with ultrapure water using a magnet to remove any remaining chemicals before they could react. Afterward, the nanocomposite was dried in a freeze-dryer for 6 h. After drying, the nanocomposite was stored in a coloured container under appropriate conditions for both further characterisation and experimental studies.

In this study, the effect of Fe_3O_4 loading rates on AE-AC was not investigated due to the reduction in magnetic properties. High loading rates can negatively affect the magnetic properties of the material, limiting the system's efficiency. Therefore, this factor was not considered in the study, leaving an area for future research.

4.2 | Apparatus and Techniques

Electrochemical analyses of capacitors designed from AE-AC and AE-AC-doped Fe_3O_4 were performed using AUTOLAB (PGSTAT128N, Nova version 2.1.5). BASi was used as a triple cell stand. These two devices were manually connected. The capacitor properties of the electrode prepared from AE-AC and AE-AC-doped Fe_3O_4 were investigated using cyclic voltammetry (CV), galvanostatic charge/discharge (GCD), and electrochemical impedance spectroscopy (EIS) techniques. EIS measurements were carried out in a 1 M H_2SO_4 electrolyte at a 10 mV AC amplitude over a frequency range of 100 kHz to 0.1 Hz at open circuit potential, under conditions where the supercapacitors were fully discharged. All electrochemical analyses were carried out in 1 M H_2SO_4 medium. Pt (MF-1032, BASi) and Ag/AgCl (Ag/AgCl, 3 M KCl; MF 2056, BASi) were used as auxiliary and reference electrodes, respectively. The supercapacitor electrode was prepared using AE-AC and AE-AC-doped Fe_3O_4, a conductivity enhancer (graphite), and mineral oil as a binder. The activated carbon, graphite, and mineral oil were mixed in a 6:2:2 ratio to form a paste, and the carbon paste was manually pressed into the electrode (MF-2010, BASi). The specific capacitance values of the supercapacitor prepared from AE-AC and AE-AC-doped Fe_3O_4 were calculated using the following equations for CV, GCD, and ESI techniques, respectively [64];

$$Cs = \frac{A}{2r\Delta V m} \text{ for CV} \tag{1}$$

$$Cs = \frac{It_d}{\Delta V m} \text{ for GCD} \tag{2}$$

$$Cs = \frac{1}{2\pi m\, fIm(Z)} \text{ for EIS} \tag{3}$$

where A, r, ΔV, m, t_d, I, f, and Im(Z) represent the electrode area, potential scan rate, potential window, active mass of the electrode material, discharge time, constant current, frequency, and imaginary impedance, respectively.

In addition, the energy and power densities of the capacitor were calculated using the data obtained with GCD using the following equations [57].

$$Es\left(\text{Wh kg}^{-1}\right) = \frac{\Delta V \times I \times t_c}{2} \text{ for energy density} \tag{4}$$

$$Ps\left(\text{Wkg}^{-1}\right) = \frac{Es}{t_d} \text{ for power density} \tag{5}$$

Acknowledgements

This work was supported in part by the Ministry of Education and Science of Ukraine (projects Nos. 0125U002005 and 0125U002033), the National Research Foundation of Ukraine (project No. 2020.02/0100), the Slovak Grant Agency VEGA (projects Nos. 2/0166/22 and 2/0131/25), and the Slovak Research and Development Agency (project No. APVV-21-0335). T.K. also acknowledges the SAIA (Slovak Academic Information Agency) for a scholarship in the Institute of Physics of the Slovak Academy of Sciences in the framework of the National Scholarship Programme of the Slovak Republic. This work has also received funding through the MSCA4Ukraine project (Grant Number 1128327), which is funded by the European Union. E.K. and O.S. acknowledge US National Science Foundation (NSF) grant CBET-2235349, including IMPRESS-U supplement, and NSF-BSF grant CBET-2422672.

Conflicts of Interest

The authors declare no conflicts of interest.

Data Availability Statement

The data that support the findings of this study are available on request.

References

1. N. Sinan and E. Unur, "Fe_3O_4/Carbon Nanocomposite: Investigation of Capacitive and Magnetic Properties for Supercapacitor Applications," *Materials Chemistry and Physics* 183 (2016): 571–579, https://doi.org/10.1016/j.matchemphys.2016.09.016.

2. E. Payami, M. A. Keynezhad, K. D. Safa, and R. Teimuri-Mofrad, "Development of High-performance Supercapacitor Based on Fe_3O_4@SiO_2@PolyFc Nanoparticles via Surface-initiated Radical Polymerization," *Electrochimica Acta* 439 (2023): 141663, https://doi.org/10.1016/j.electacta.2022.141663.

3. <number>[3]/number>W. Raza, F. Ali, N. Raza, et al., "Recent Advancements in Supercapacitor Technology," *Nano Energy* 52 (2018): 441–473, https://doi.org/10.1016/j.nanoen.2018.08.013.

4. A. Levent and C. Saka, "Enhanced Electrochemical Performance of ZnO@Sulphur-doped Carbon Particles for Use in Supercapacitors," *Journal of Energy Storage* 78 (2024): 110120, https://doi.org/10.1016/j.est.2023.110120.

5. C. Saka and A. Levent, "Fabrication of Nitrogen and ZnO Doped on Carbon Particles Obtained From Waste Biomass and Their Use as Supercapacitor Electrodes for Energy Storage," *International Journal of Hydrogen Energy* 90 (2024): 1070–1083, https://doi.org/10.1016/j.ijhydene.2024.10.061.

6. A. Levent and C. Saka, "Mesoporous Carbon Particles by Biomass Waste Based on Sulfonation and Copper Oxide Functionalization as Efficient and Stable Electrode Material for Supercapacitor," *Environmental Science and Pollution Research* 31, no. 39 (2024): 52511–52522, https://doi.org/10.1007/s11356-024-34710-y.

7. R. Fan, C. Zhao, J. Ma, et al., "Boosting Reaction Kinetics and Improving Long Cycle Life in Lamellar VS_2/MoS_2 Heterojunctions for Superior Sodium Storage Performance," *Journal of Materials Chemistry A* 10, no. 2 (2022): 939–949, https://doi.org/10.1039/D1TA09612E.

8. Z. Yu, L. Tetard, L. Zhai, and J. Thomas, "Supercapacitor Electrode Materials: Nanostructures From 0 to 3 Dimensions," *Energy and Environmental Science* 8, no. 3 (2015): 702–730, https://doi.org/10.1039/C4EE03229B.

9. C. Tu, X. Li, C. Lu, Q. Luo, T. Li, and M. Zhu, "A Sequential Process to Synthesize Fe_3O_4@MnO_2 Hollow Nanospheres for High Performance Supercapacitors," *Materials Chemistry Frontiers* 6, no. 14 (2022): 1938–1947, https://doi.org/10.1039/D2QM00450J.

10. T. H. Yun, T. Kim, Y. Hwang, et al., "Laser-Assisted Rapid Fabrication of Cobalt Hydroxide@Carbon Fiber Composites for High-Performance, Robust Structural Supercapacitors," *ACS Applied Energy Materials* 7, no. 21 (2024): 10120–10133, https://doi.org/10.1021/acsaem.4c02261.

11. P. Xiao, M. Shi, L. Xu, et al., "An Efficient Chemical Reduction-Induced Assembly of Fe_3O_4@ Graphene Fiber for Wire-Shaped Supercapacitors With Ultrahigh Volumetric Energy Density," *Science China Technological Sciences* 64, no. 10 (2021): 2246–2254, https://doi.org/10.1007/s11431-020-1896-5.

12. I. Bordun and E. Szymczykiewicz, "Synthesis and Electrochemical Properties of Fe_3O_4/C Nanocomposites for Symmetric Supercapacitors," *Applied Sciences* 14, no. 2 (2024): 677, https://doi.org/10.3390/app14020677.

13. M. G. Tadesse, E. Kasaw, and J. F. Lübben, "Valorization of Banana Peel Using Carbonization: Potential Use in the Sustainable Manufacturing of Flexible Supercapacitors," *Micromachines* 14, no. 2 (2023): 330, https://doi.org/10.3390/mi14020330.

14. G. S. Dos Reis, S. H. Larsson, H. P. de Oliveira, M. Thyrel, and E. Claudio Lima, "Sustainable Biomass Activated Carbons as Electrodes for Battery and Supercapacitors—A Mini-Review," *Nanomaterials* 10, no. 7 (2020): 1398, https://doi.org/10.3390/nano10071398.

15. A. Tundwal, H. Kumar, B. J. Binoj, et al., "Developments in Conducting Polymer-, Metal Oxide-, and Carbon Nanotube-based Composite Electrode Materials for Supercapacitors: A Review," *RSC Advances* 14, no. 14 (2024): 9406–9439, https://doi.org/10.1039/D3RA08312H.

16. A. Muzaffar, M. B. Ahamed, and C. M. Hussain, "Green Supercapacitors: Latest Developments and Perspectives in the Pursuit of Sustainability," *Renewable and Sustainable Energy Reviews* 195 (2024): 114324, https://doi.org/10.1016/j.rser.2024.114324.

17. M. Sathyan, P. J. Jandas, M. Venkatesan, S. C. Pillai, and H. John, "Electrode Material for High Performance Symmetric Supercapacitors Based on Superparamagnetic Fe_3O_4 Nanoparticles Modified With Cetyltrimetylammonium Bromide," *Synthetic Metals* 287 (2022): 117080, https://doi.org/10.1016/j.synthmet.2022.117080.

18. Q. Wang, L. Jiao, H. Du, Y. Wang, and H. Yuan, "Fe_3O_4 Nanoparticles Grown on Graphene as Advanced Electrode Materials for Supercapacitors," *Journal of Power Sources* 245 (2014): 101–106, https://doi.org/10.1016/j.jpowsour.2013.06.035.

19. X. Zhang, K. Y. Zhao, S. Su, Z. L. Zou, Y. Q. Qian, and K. Cheng, "Construction of Sandwich-Structured Co_3O_4–Fe_3O_4 Composite Electrode With Free Binder for High-Performance All-Solid-State Supercapacitor," *Rare Metals* 44 (2025): 1–6, https://doi.org/10.1007/s12598-017-0925-6.

20. L. Li, P. Gao, S. Gai, et al., "Ultra Small and Highly Dispersed Fe_3O_4 Nanoparticles Anchored on Reduced Graphene for Supercapacitor Application," *Electrochimica Acta* 190 (2016): 566–573, https://doi.org/10.1016/j.electacta.2015.12.137.

21. H. A. Ghaly, A. G. El-Deen, E. R. Souaya, and N. K. Allam, "Asymmetric Supercapacitors Based on 3D Graphene-wrapped V_2O_5 Nanospheres and Fe_3O_4@3D Graphene Electrodes With High Power and Energy Densities," *Electrochimica Acta* 310 (2019): 58–69, https://doi.org/10.1016/j.electacta.2019.04.071.

22. I. Y. Bu and R. Huang, "Fabrication of CuO-decorated Reduced Graphene Oxide Nanosheets for Supercapacitor Applications," *Ceramics International* 43, no. 1 (2017): 45–50, https://doi.org/10.1016/j.ceramint.2016.08.136.

23. Y. Zhang, Y. Hu, Z. Wang, et al., "Lithiation-induced Vacancy Engineering of Co_3O_4 With Improved Faradic Reactivity for High-Performance Supercapacitor," *Advanced Functional Materials* 30, no. 39 (2020): 2004172, https://doi.org/10.1002/adfm.202004172.

24. T. Prasankumar, B. R. Wiston, C. R. Gautam, R. Ilangovan, and S. P. Jose, "Synthesis and Enhanced Electrochemical Performance of PANI/Fe_3O_4 Nanocomposite as Supercapacitor Electrode," *Journal of Alloys and Compounds* 757 (2018): 466–475, https://doi.org/10.1016/j.jallcom.2018.05.108.

25. A. K. Singh, N. Deepak, S. Shukla, and S. Saxena, "V_2O_5 Nanoribbons for Improved Cyclic Stability in Aqueous K^+-ions Based Supercapacitor," *Emergent Materials* 8 (2025): 3603–3614, https://doi.org/10.1007/s42247-024-00915-7.

26. T. Akila, G. A. Sibu, P. Gayathri, and V. Balasubramani, "Enhanced Cycling Rate Performance of Three-dimensional NiO as a Positive Electrode for Hybrid Supercapacitor," *Journal of Materials Science* 59, no. 19 (2024): 8360–8373, https://doi.org/10.1007/s10853-024-09650-0.

27. J. Chen, J. Qiu, B. Wang, H. Feng, K. Ito, and E. Sakai, "Fe_3O_4/Biocarbon Composites With Superior Performance in Supercapacitors," *Journal of Electroanalytical Chemistry* 804 (2017): 232–239, https://doi.org/10.1016/j.jelechem.2017.09.028.

28. J. Yu, Y. Qian, X. Ma, et al., "Preparation of β-$Co(OH)_2$ Nanosheets for Pseudocapacitive Electrode via Cathode Glow Discharge Electrolysis," *Journal of Sol-Gel Science and Technology* 109, no. 2 (2024): 555–568, https://doi.org/10.1007/s10971-023-06297-2.

29. X. Yi, H. Sun, N. Robertson, and C. Kirk, "Nanoflower $Ni(OH)_2$ Grown in Situ on Ni Foam for High-performance Supercapacitor Electrode Materials," *Sustain Energy Fuels* 5, no. 20 (2021): 5236–5246, https://doi.org/10.1039/D1SE01036K.

30. X. Lv, Y. Zhang, L. Wen, A. Yang, and J. Liang, "Facile Synthesis of Fe_3O_4 Ultrathin Layer Coated Fe_2O_3 Composite Anode for Enhanced

Lithium-ion Storage," *Journal of Electroanalytical Chemistry* 947 (2023): 117758, https://doi.org/10.1016/j.jelechem.2023.117758.

31. J. Song, T. Liu, Y. He, et al., "Engineering Semicoherent Interface With O–Fe–Se Coordination for Boosting the Capacity and Rate Capability of a Battery-type Supercapacitor Anode," *Science China Chemistry* 66, no. 5 (2023): 1767–1778, https://doi.org/10.1007/s40843-022-2330-6.

32. E. Pameté, L. Köps, F. A. Kreth, et al., "The Many Deaths of Supercapacitors: Degradation, Aging, and Performance Fading," *Advanced Energy Materials* 13, no. 29 (2023): 2301008, https://doi.org/10.1002/aenm.202301008.

33. W. Zhang, P. Yang, H. Wang, S. Sun, and S. Yao, "Preparation and Characterization of High-performance Fe_3O_4/RGO Anode for Supercapacitors," *Journal of Electronic Materials* 52, no. 9 (2023): 6107–6120, https://doi.org/10.1007/s11664-023-10552-1.

34. S. K. Park, J. Sure, D. S. M. Vishnu, et al., "Nano-Fe_3O_4/Carbon Nanotubes Composites by One-pot Microwave Solvothermal Method for Supercapacitor Applications," *Energies* 14, no. 10 (2021): 2908, https://doi.org/10.3390/en14102908.

35. E. R. Kenawy, Y. I. Moharram, F. S. Abouharga, and M. Elfiky, "Electrospun Polyacrylonitrile-polyphenyl/Magnetite Nanofiber Electrode for Enhanced Capacitance of Supercapacitor," *Scientific Reports* 15, no. 1 (2025): 14885, https://doi.org/10.1038/s41598-025-97089-x.

36. S. S. Hegde and B. R. Bhat, "Sustainable Energy Storage: *Mangifera Indica* Leaf Waste-Derived Activated Carbon for Long-Life, High-Performance Supercapacitors," *RSC Advances* 14, no. 12 (2024): 8028–8038, https://doi.org/10.1039/D3RA08910J.

37. M. Zielińska and K. Bułkowska, "Agricultural Wastes and Their By-Products for the Energy Market," *Energies* 17, no. 9 (2024): 2099, https://doi.org/10.3390/en17092099.

38. R. Kumar, R. K. Nekouei, and V. Sahajwalla, "In-situ Carbon-coated Iron Oxide (ISCC-Fe_3O_4) as an Efficient Electrode Material for Supercapacitor Applications," *Ceramics International* 51, no. 9 (2025): 12312–12320, https://doi.org/10.1016/j.ceramint.2025.01.071.

39. G. H. Al-Hazmi, H. A. Saad, M. S. Refat, and A. M. A. Adam, "Fe_3O_4-Carbon-based Composite Derived From the Charge-Transfer Reaction Using Waste Tea Leaves as the Carbon Precursor for Enhanced Removing of Azocarmine G2, Methyl Violet 2B, Eosin B, and Toluidine Blue From Aqueous Solution," *Crystals* 12, no. 10 (2022): 1355, https://doi.org/10.3390/cryst12101355.

40. I. Lestari, A. V. Yohana, F. Farid, and D. R. Gusti, "Preparation and Characterisation of Composite Magnetite Fe_3O_4-activated Carbon as Adsorben of Phenol," *Jurnal Riset Kimia* 13, no. 1 (2022): 34–48, https://doi.org/10.25077/jrk.v13i1.442.

41. R. Foroutan, S. J. Peighambardoust, S. H. Peighambardoust, M. Pateiro, and J. M. Lorenzo, "Adsorption of Crystal Violet Dye Using Activated Carbon of Lemon Wood and Activated Carbon/Fe_3O_4 Magnetic Nanocomposite From Aqueous Solutions: A Kinetic, Equilibrium and Thermodynamic Study," *Molecules* 26, no. 8 (2021): 2241, https://doi.org/10.3390/molecules26082241.

42. P. Yin, Y. Deng, L. Zhang, et al., "Facile Synthesis and Microwave Absorption Investigation of Activated Carbon@Fe_3O_4 Composites in the Low Frequency Band," *RSC Advances* 8, no. 41 (2018): 23048–23057, https://doi.org/10.1039/C8RA04141E.

43. P. L. Hariani, M. Faizal, and D. Setiabudidaya, "Removal of Procion Red MX-5B From Songket's Industrial Wastewater in South Sumatra Indonesia Using Activated Carbon-Fe_3O_4 Composite," *Sustainable Environment Research* 28, no. 4 (2018): 158–164, https://doi.org/10.1016/j.serj.2018.01.004.

44. P. Saini, J. K. Yadav, B. Rani, A. P. Pandey, and A. Dixit, "High-Performance Symmetric Supercapacitor Using Cost-efficient Iron Oxide (Fe_3O_4) Nanoparticles," *Energy Storage* 6, no. 2 (2024): e608, https://doi.org/10.1002/est2.608.

45. C. Zhao, X. Shao, Y. Zhang, and X. Qian, "Fe_2O_3/RGO/Fe_3O_4 Composite in Situ Grown on Fe Foil for High Performance Supercapacitors," *ACS Applied Materials and Interfaces* 8, no. 44 (2016): 30133–30142, https://doi.org/10.1021/acsami.6b09594.

46. I. I. G. Inal, S. M. Holmes, A. Banford, and Z. Aktas, "The Performance of Supercapacitor Electrodes Developed From Chemically Activated Carbon Produced From Waste Tea," *Applied Surface Science* 357, no. Pt A (2015): 696–703, https://doi.org/10.1016/j.apsusc.2015.09.067.

47. H. Aydın, Ü. Kurtan, B. Üstün, S. N. Koc, E. Akgül, and M. Demir, "A Review on the Recent Advancement of Metal-boride Derived Nanostructures for Supercapacitors," *Journal of Energy Storage* 72, no. Pt A (2023): 108306, https://doi.org/10.1016/j.est.2023.108306.

48. S. Zhang and N. Pan, "Supercapacitors Performance Evaluation," *Advanced Energy Materials* 5, no. 6 (2015): 1401401, https://doi.org/10.1002/aenm.201401401.

49. J. Gamby, P. L. Taberna, P. Simon, J. F. Fauvarque, and M. Chesneau, "Studies and Characterisations of Various Activated Carbons Used for Carbon/Carbon Supercapacitors," *Journal of Power Sources* 101, no. 1 (2001): 109–116, https://doi.org/10.1016/S0378-7753(01)00707-8.

50. R. Farma, M. Deraman, I. A. Talib, et al., "Physical and Electrochemical Properties of Supercapacitor Electrodes Derived From Carbon Nanotube and Biomass Carbon," *International Journal of Electrochemical Science* 8, no. 1 (2013): 257–273, https://doi.org/10.1016/S1452-3981(23)14018-1.

51. K. Aruchamy, R. Nagaraj, H. M. Manohara, et al., "One-step Green Route Synthesis of Spinel $ZnMn_2O_4$ Nanoparticles Decorated on MWCNTs as a Novel Electrode Material for Supercapacitor," *Materials Science and Engineering B* 252 (2020): 114481, https://doi.org/10.1016/j.mseb.2019.114481.

52. M. S. Gouda, M. Shehab, S. Helmy, M. Soliman, and R. S. Salama, "Nickel and Cobalt Oxides Supported on Activated Carbon Derived From Willow Catkin for Efficient Supercapacitor Electrode," *Journal of Energy Storage* 61 (2023): 106806, https://doi.org/10.1016/j.est.2023.106806.

53. P. Ozpinar, C. Dogan, H. Demiral, et al., "Activated Carbons Prepared From Hazelnut Shell Waste by Phosphoric Acid Activation for Supercapacitor Electrode Applications and Comprehensive Electrochemical Analysis," *Renewable Energy* 189 (2022): 535–548, https://doi.org/10.1016/j.renene.2022.02.126.

54. A. Adan-Mas, L. Alcaraz, P. Arévalo-Cid, F. A. López-Gómez, and F. Montemor, "Coffee-derived Activated Carbon From Second Biowaste for Supercapacitor Applications," *Waste Management* 120 (2021): 280–289, https://doi.org/10.1016/j.wasman.2020.11.043.

55. C. J. Raj, R. Manikandan, M. Rajesh, et al., "Cornhusk Mesoporous Activated Carbon Electrodes and Seawater Electrolyte: The Sustainable Sources for Assembling Retainable Supercapacitor Modüle," *Journal of Power Sources* 490 (2021): 229518, https://doi.org/10.1016/j.jpowsour.2021.229518.

56. C. H. Xu, P. Y. Shen, Y. F. Chiu, et al., "Atmospheric Pressure Plasma Jet Processed Nanoporous Fe_2O_3/CNT Composites for Supercapacitor Application," *Journal of Alloys and Compounds* 676 (2016): 469–473, https://doi.org/10.1016/j.jallcom.2016.03.185.

57. D. Guan, Z. Gao, W. Yang, et al., "Hydrothermal Synthesis of Carbon Nanotube/Cubic Fe_3O_4 Nanocomposite for Enhanced Performance Supercapacitor Electrode Material," *Materials Science and Engineering: B* 178, no. 10 (2013): 736–743, https://doi.org/10.1016/j.mseb.2013.03.010.

58. M. A. A. Mariah, K. Rovina, J. M. Vonnie, and K. H. Erna, "Characterization of Activated Carbon From Waste Tea (*Camellia sinensis*) Using Chemical Activation for Removal of Methylene Blue and Cadmium Ions," *South African Journal of Chemical Engineering* 44 (2023): 113–122, https://doi.org/10.1016/j.sajce.2023.01.007.

59. H. Khurshid, M. R. U. Mustafa, and M. H. Isa, "Modified Activated Carbon Synthesized From Oil Palm Leaves Waste as a Novel Green Adsorbent for Chemical Oxygen Demand in Produced Water," *Sustainability* 14, no. 4 (2022): 1986, https://doi.org/10.3390/su14041986.

60. R. Vinayagam, M. Quadras, T. Varadavenkatesan, et al., "Magnetic Activated Carbon Synthesized Using Rubber Fig Tree Leaves for Adsorp-

tive Removal of Tetracycline From Aqueous Solutions," *Environmental Research* 216, no. Pt 3 (2023): 114775, https://doi.org/10.1016/j.envres.2022.114775.

61. M. Güneş, E. Ertaş, S. Tumur, et al., "Synthesis and Antibacterial Evaluation of Silver-coated Magnetic Iron Oxide/Activated Carbon Nanoparticles Derived From *Hibiscus esculentus*," *Magnetochemistry* 11, no. 7 (2025): 53, https://doi.org/10.3390/magnetochemistry11070053.

62. T. S. Saleh, A. K. Badawi, R. S. Salama, and M. M. M. Mostafa, "Design and Development of Novel Composites Containing Nickel Ferrites Supported on Activated Carbon Derived From Agricultural Wastes and Its Application in Water Remediation," *Materials* 16, no. 6 (2023): 2170, https://doi.org/10.3390/ma16062170.

63. A. H. Birniwa, R. E. A. Mohammad, M. Ali, et al., "Synthesis of Gum Arabic Magnetic Nanoparticles for Adsorptive Removal of Ciprofloxacin: Equilibrium, Kinetic, Thermodynamics Studies, and Optimization by Response Surface Methodology," *Separations* 9, no. 10 (2022): 322, https://doi.org/10.3390/separations9100322.

64. S. Ratha and A. K. Samantara, *Supercapacitor: Instrumentation, Measurement and Performance Evaluation Techniques* (Springer: Singapore, 2018), 30–40, https://doi.org/10.1007/978-981-13-3086-5.